# Nonequilibrium Liquid–Liquid Phase Separation in Crystallizable Polymer Solutions

**Hwan K. Lee,† Allan S. Myerson,† and Kalle Levon*,‡**

*Department of Chemical Engineering and Department of Chemistry, Polytechnic University, 333 Jay Street, Brooklyn, New York 11201*

*Received December 3, 1991; Revised Manuscript Received April 16, 1992*

ABSTRACT: The relation between liquid–liquid phase separation and crystallization was investigated by applying a systematic change in the interaction in isotactic polypropylene (i-PP) solutions with a proper selection of solvents. A series of dialkyl phthalates, with a different number of carbon atoms in the alkyl chain, was used to control the solvent quality. The liquid–liquid phase separation temperature decreased remarkably when the interaction became favorable while the melting point curve remained constant. As the result of this systematic change in polymer–solvent interaction, the liquid–liquid phase separation was observed under nonequilibrium conditions below the equilibrium liquid–solid transition. Liquid–liquid phase separation of the i-PP solutions with strong interaction was probed by using atactic polypropylene (a-PP) in the same solvent systems. The results indicate that although the liquid–liquid phase separation of i-PP solutions with the strong interactions cannot be observed in situ due to the competing crystallization, liquid demixing can occur at a low temperature during rapid quenching. An additional feature oberved under the nonequilibrium conditions was liquid–liquid phase separation induced by crystallization in concentration and temperature regions outside the binodal curve. In polydisperse samples, fractionation during liquid–liquid phase separation resulted in bimodal behavior of the liquid–liquid transition and in deviation of melting points in the biphasic region.

## Introduction

The complexity of multiphase structures formed from polymer–solvent mixtures has resulted in the description of structure-property relationships. To understand their complex structures, the overall concept of equilibrium behavior and the kinetics of nonequilibrium competition between possible phase separations should be related to the properties of the final product. Recently, a wide interest has arisen in a thermally induced phase separation (TIPS) process where liquid–liquid phase separation competes with crystallization. The TIPS process has been applied to produce membranes,[1] liquid–crystal displays,[2] and low-density materials.[3]

The equilibrium phase behavior of a polymer–solvent mixture, in which both crystallization and liquid–liquid phase separation may occur, was presented by Richards[4] in the 1940s. This was followed by experimental data from several research groups[5] for representative polymer–solvent pairs. In all of these systems, the upper critical solution temperature (UCST) locates above the melting point curve. The liquid–liquid phase separation can easily be identified on cooling by cloud point measurements and the crystallization can similarly be detected by light scattering between crossed polars. The final morphology depends on the nonequilibrium conditions and composition, and both influence the kinetics of liquid–liquid phase separation and crystallization. Liquid–liquid phase separation may occur either by nucleation and growth or by spinodal decomposition, and crystallization occurs by nucleation and growth mechanisms.

The influence of molecular weight on the phase behavior was investigated by Koningsveld[6] over 20 years ago. A decrease in molecular weight lowered the UCST, but the melting point depression was essentially unaffected. This phenomena resulted in phase behavior where the UCST lies below the melting temperatures. Such a liquid–liquid phase separation has no equilibrium significance but would have a significant influence on the final morphology under nonequilibrium conditions, where liquid–liquid phase separation would be able to precede crystallization due to the high nucleation barrier to polymer crystallization. After Koningsveld's calculations very little interest has been focused on the above mentioned nonequilibrium liquid–liquid phase separation. Experimental results showing the molecular weight effects on the phase behavior supporting Koningsveld's calculations were recently presented by Chiu and Mandelkern.[7] Burghardt[8] calculated the effects of interactions on the phase behavior in semicrystalline polymer systems and predicted the existence of nonequilibrium liquid–liquid phase transition. Papkov[9] has shown the existence of UCST below equilibrium liquid–solid transition, but his experimental results actually represent a situation of a ternary system where phase separation is induced by a nonsolvent.

Structure formation by liquid–liquid phase separation and crystallization in polymer blends has been investigated in a few cases.[10-12] Inaba et al.[10] established a morphology control in a mixture of isotactic polypropylene (i-PP) and ethylene–propylene random copolymer (EPR) through spinodal decomposition and crystallization. They were able to lock-in the modulated structure resulting from liquid–liquid phase separation by the crystallization process. The conservation of the modulated structure was achieved when the crystallization rate is rapid enough to suppress segregation of EPR from the crystallizing front of i-PP. In this case, the crystallization can be characterized as the linear growth of spherulite size with time. Tanaka and Nishi[11] observed a local phase separation at the growth front of a spherulite in a binary blend of poly(ϵ-caprolactone) and polystyrene oligomer when the composition and thermal conditions were outside the binodal curve. They concluded that the local phase separation is responsible for high mobility of diluent (polystyrene oligomer) during crystallization, resulting in a nonlinear growth of spherulite with time. In all these systems, the UCST exists above the melting point.

In this paper, we report the effects of interaction between polymer and solvent and of molecular weight of polymer

* To whom the correspondence should be addressed.
† Department of Chemical Engineering.
‡ Department of Chemistry.

0024-9297/92/2225-4002$03.00/0 

Table I
Molecular Characteristics, Vapor Pressure, and Supplier of Phthalates

| symbol | alkyl group | $M_w$ | bp (°C)/ pressure (mmHg)[a] | supplier |
|---|---|---|---|---|
| $C_4$ | butyl | 278 | 340/760 | Aldrich |
| $C_6$ | hexyl | 334 | 210/5 | Exxon |
| $C_7$ | heptyl | 362 | 220/5 | Exxon |
| $C_8$ | octyl | 391 | 230/5 | Exxon |
| $C_{8b}$ | 2-ethylhexyl | 391 | 390/760 | Aldrich |
| $C_9$ | nonyl | 419 | 251/5 | Exxon |
| $C_{10}$ | decyl | 447 | 256/5 | Exxon |

[a] From the information provided by the suppliers.

on the phase behavior by using isotactic polypropylene (i-PP) and dialkyl phthalate as a solvent. The variation of the number of carbon atoms in the alkyl substituent of phthalate is utilized to control the solvent power. The overall purpose of this research is to establish a polymer–solvent pair with which the liquid–liquid phase separation cannot be observed at the equilibrium state but can be measured by optical methods in situ with reasonably slow cooling rates. We will also explore the liquid–liquid phase separation of the system with strong interaction in which liquid–liquid phase separation cannot be observed in situ due to competing crystallization. In order to exclude interference by crystallization, atactic polypropylene (a-PP) will be used instead of i-PP with the same solvent systems.

## Experimental Section

**Materials.** Isotactic polypropylene (i-PP) used in this investigation was commercial grade (Exxon PD020; $M_w$ 4.4 × $10^5$, $M_w/M_n$ 6.8), and three fractions, designated L-MW, M-MW, and H-MW, with the following molecular characteristics (1) L-MW ($M_w$ 1.2 × $10^5$, $M_w/M_n$ 2.5), (2) M-MW ($M_w$ 3.1 × $10^5$, $M_w/M_n$ 3.4), (3) H-MW ($M_w$ 7.0 × $10^5$) were supplied by Himont R&D center. Atactic polypropylene (a-PP)[13] with $M_w$ = 3.8 × $10^5$ and $M_w/M_n$ = 1.1 was obtained from Exxon Research and Engineering Co.

The solvents were series of 1,2-dialkyl phthalates with the different number of carbon atoms in the alkyl chain, designated as $C_4$, $C_6$, $C_7$, $C_8$, $C_{8b}$, $C_9$, and $C_{10}$. Molecular characteristics such as the type of alkyl group and molecular mass, vapor pressure, and supplier are summarized in Table I.

**Preparation Method I.** i-PP pellets were dissolved to obtain known concentrations (30–60 wt %) in the solvent containing a few ppm of an antioxidant (2,6-di-*tert*-butyl-4-methylphenol). i-PP solution films were prepared at 200–210 °C with a thickness of 100–300 μm in nitrogen medium, and the concentrations were reconfirmed by extracting the solvents with hexane. An additional amount of solvent was introduced to the resulting films to vary the concentration of the specimen in concavity microslides for optical microscope observation.

**Preparation Method II.** The dried thin films (20–40 μm) were cast according to the following procedure: i-PP powder was dissolved in hot decalin containing 2,6-di-*tert*-butyl-4-methylphenol (0.5% w/w on polymer) under nitrogen to form 0.7–1.0% w/w solutions; temperatures were close to the solvent boiling point; the solutions were held under reflux for 30 min after dissolution; the hot solutions were quenched by pouring them into an aluminum tray in an ice–water bath; the bulk of the solvent was allowed to evaporate in a current of air under ambient conditions, and a transparent film was obtained; the residual solvent was removed by extraction with methanol; the films were dried in vacuum. a-PP films were obtained similarly by using xylene. a-PP was easily dissolved in xylene at room temperature. Solutions of known concentration were prepared in concavity microslides.

Since both preparation methods allowed the same results in optical microscopy with the polydisperse sample, the solutions of fractionated i-PP and a-PP were prepared according to Method II.

**Phase Transition Temperature Determination.** Observation of liquid–liquid phase separation temperature ($T_{L-L}$) was followed by optial microscopy (Nikon HFX II) in a modulation contrast (Hoffman modulation contrast). Melting point ($T_m$) and crystallization temperature ($T_{cry}$) were observed through optical microscopy between cross polars in transmitted light. Thermal treatments were done in a Mettler hotstage (FP82) and controller (FP80). The samples were slowly heated to 10 °C above the higher value of either the melting point or liquid–liquid phase separation temperature. The heating was continued for 10 min to ensure the homogeneous state. The cooling and heating rates for the measurement of the phase transition temperatures were 10, 2, and 0.5 °C/min. Evaporation of solvents was checked by weighing the system after running and was neglible except $C_4$ in the experimental ranges.

For DSC specimen preparation, i-PP powder (6–7 mg) and solvent were sealed in stainless steel pans with O-rings and dissolved at 190 °C for 10 min. The melting points (extrapolated) and the crystallization temperatures (onset) were measured by DSC (Perkin-Elmer DSC-7 instrument) at a rate of 10 °C/min.

The melting points and crystallization temperatures were measured by DSC for the polydisperse polymer solutions and by optical microscopy for the fractionated i-PP samples. The differences in the obtained values due to the different methods can mainly be attributed to the heat transfer and heat evolution process and do not affect the general features discussed in this manuscript. We did not use cloud point measurements because they are not able to distinguish liquid–liquid phase separation and crystallization when the two transitions are close together.

## Results and Discussion

**Systematic Change in Interaction.** The liquid–liquid transitions and the crystallization temperatures, both observed on the cooling cycle (cooling rate 10 °C/min) for H-MW with $C_6$, $C_7$, and $C_8$ solvents, are presented in Figure 1. In addition, the melting temperatures, which are determined on a heating cycle (heating rate 10 °C/min), are included in this figure. The observed transitions are by no means equilibrium transitions, since nonequilibrium phenomena may be involved. The liquid–liquid phase transition at 3–10 wt % for the H-MW/$C_6$ pair is located above the melting temperatures similar to the classical example presented by Richards.[4] The liquid–liquid phase separation between 10 and 40 wt % occurs below the melting temperatures prior to crystallization. This part of the liquid–liquid transition is clearly of nonequilibrium nature. The observation of the phase transition depends on the cooling conditions and will be discussed later. The modulated structure resulting from liquid–liquid phase separation observed at 135 °C for 10 wt % polymer concentration with Hoffman modulation contrast (HMC) is shown in Figure 2a. The same sample shows clearly both the spherulitic crystal under crossed polars and the modulated structure on the surface when crystallized at 100 °C for 10 min (Figure 2b,c; note that the two micrographs were obtained on the same field of the sample).

With a better solvent, $C_7$, the liquid–liquid phase separation temperatures shift below the melting points on the whole concentration region including the highest temperature at which the liquid demixing is observed (Figure 1b). This is to our knowledge the first demonstration for the existence of a nonequilibrium liquid–liquid transition in polyolefins as a result of a systematic change in the interaction, as predicted by Burghardt.[8] The highest temperature for this liquid–liquid phase separation decreased further when a better solvent, $C_8$, was used (Figure 1c). The logical extension of the systematic change in interaction would be observation of a liquid–liquid phase separation at low temperatures using $C_9$ as the solvent. We were not able to observe liquid demixing for the

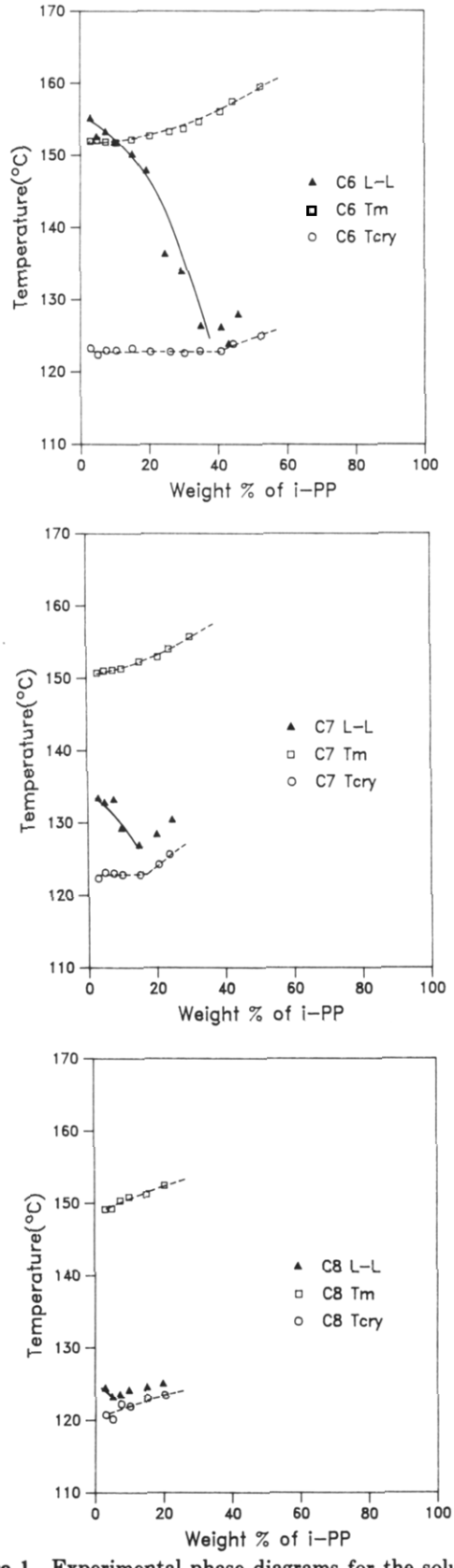


**Figure 1.** Experimental phase diagrams for the solutions of H-MW i-PP and $C_6$ (a, top) $C_7$ (b, middle), and $C_8$ (c, bottom) phthalates.

H-MW/$C_9$ pair before crystallization at a cooling rate of 10 °C/min. Figure 3 shows the spherulitic crystal structure for H-MW/$C_9$ (2.5 wt %) formed at 100 °C. The volume-filling spherulites are observed under cross polars in contrast to the deteriorated spherulites in Figure 2b. No evidence of liquid–liquid phase separation can be seen

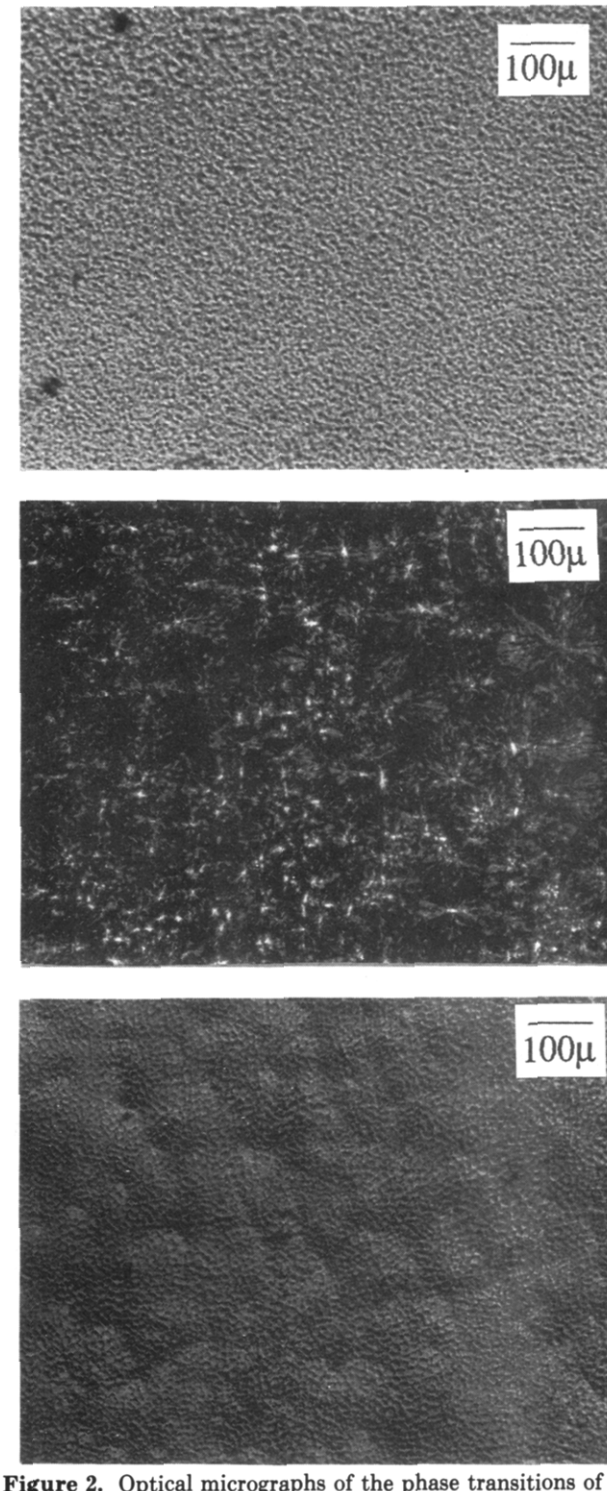


**Figure 2.** Optical micrographs of the phase transitions of H-MW i-PP/$C_6$ (polymer concentration 10 wt %): (a, top) liquid–liquid phase transition observed with Hoffman modulation contrast (HMC) before crystallization at 135 °C; (b, middle) spherulitic crystalline structures observed under crossed polars, cooled to 100 °C at 10 °C/min and held for 10 min; (c, bottom) picture obtained by HMC on the same field of the sample in (b).

with HMC (Figure 3b). Since crystallization occurs first under the thermal conditions applied, liquid–liquid phase separation cannot be observed in situ.

**Molecular Weight Effects.** The change in polymer molecular weight is known to have an influence on the phase transitions.[6,7] The phase transitions for M-MW/$C_6$ and -$C_7$ pairs, as shown in Figure 4, were obtained at 10 °C/min rates of cooling and heating. The liquid–liquid phase transition temperatures are slightly lower than those

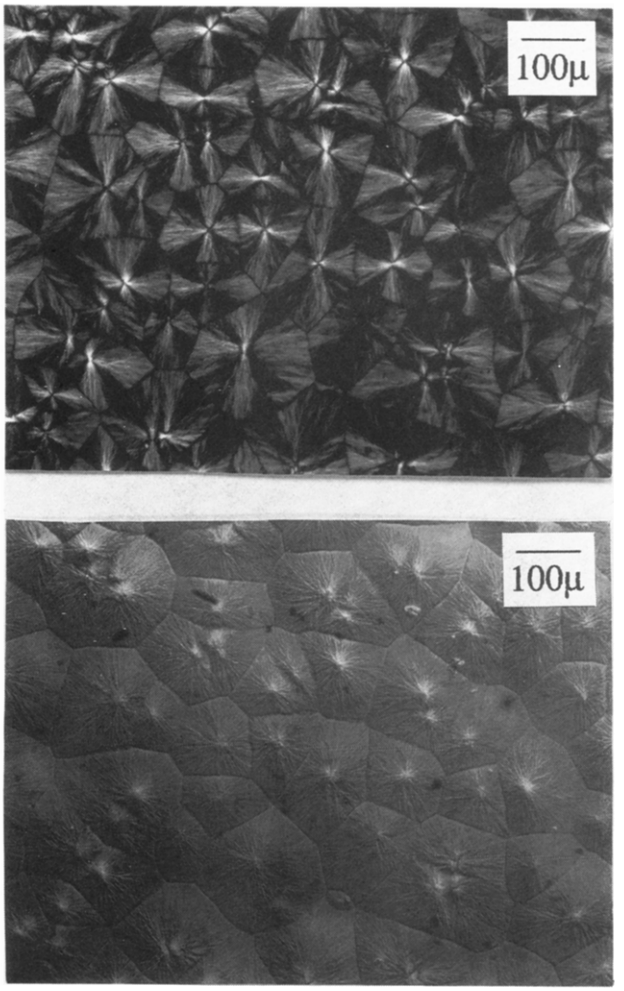


**Figure 3.** Optical micrographs of H-MW i-PP/$C_9$ (polymer concentration 2.5 wt %), cooled to 100 °C at 10 °C/min and held for 10 min: spherulitic structure under crossed polars (a, top) and with HMC (b, bottom).

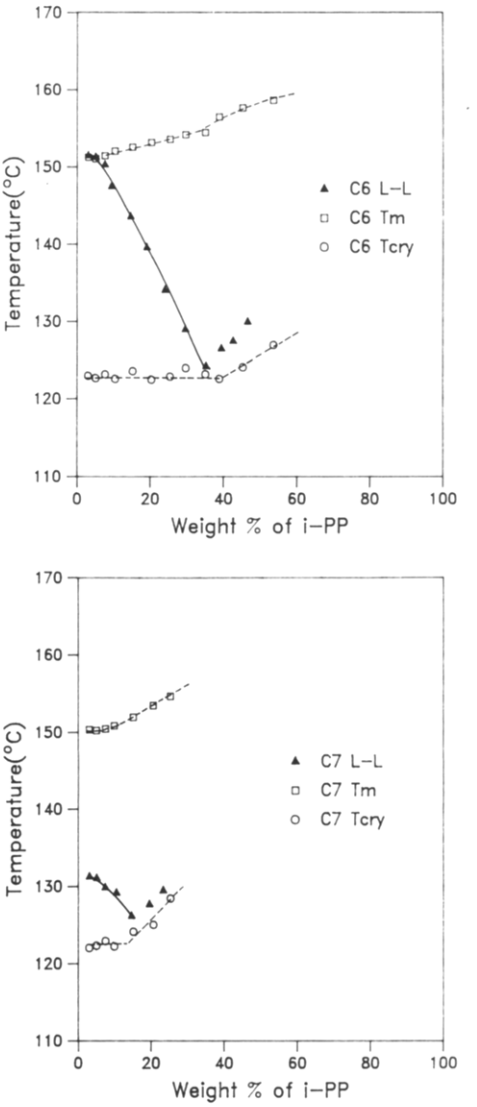


**Figure 4.** Experimental phase diagrams for the solutions of M-MW i-PP and $C_6$ (a, top) and $C_7$ (b, bottom) phthalates.

of the H-MW fractions with the same solvents (Figure 1), reflecting the difference in the molecular weights of these two samples. An interesting result was observed with the M-MW/$C_8$ pair. A liquid–liquid phase separation could not be observed before crystallization even at the low polymer concentrations. Thus the liquid–liquid decomposition is pushed below crystallization temperature with $C_8$ when the polymer molecular weight was decreased. Similar effects were observed with L-MW with which liquid–liquid separation cannot be measured using $C_7$ as the solvent (Figure 5b). Additionally, the highest liquid–liquid phase separation temperature for the L-MW i-PP/$C_6$ pair, as seen in Figure 5a, is lower than for H-MW and M-MW fractions.

The molecular weight effects on the two transitions are presented in Figure 6. When $C_6$ was used as the solvent, at about 5 wt % concentrations, the liquid–liquid transition lies above the melting transition in the case of the H-MW fraction, coincides with the $T_m$ value when M-MW is used, and then finally moves clearly below the melting transition with L-MW. The decreasing UCST with the decreasing molecular weight can be explained by the increasing entropy in the system. The melting temperature of L-MW is greater than those of M-MW and H-MW. This melting point inversion can be related to the kinetics of chain-folded crystal formation. The chain packing is retarded in the H-MW and M-MW fractions due to low mobility of the long chain molecules, resulting in formation of a thin lamella. Similar results were reported by Chiu and Mandelkern.[7]

The effects of solvent quality and polymer molecular weight on phase transitions are summarized in Table II. In all cases with $C_9$ solvent, liquid–solid transition was first observed during cooling. The last (or most favorable) solvent with which the liquid–liquid transition can be observed prior to entering liquid–solid transition at a cooling rate of 10 °C/min is different for each fractionated sample: $C_8$ for H-MW, $C_7$ for M-MW, and $C_6$ for L-MW.

**Liquid–Liquid Phase Separation Induced by Crystallization.** A striking feature in Figures 1, 4, and 5 is the rise of liquid–liquid phase transition at high concentrations outside the binodal curve. In the M-MW/$C_6$ system (Figure 4a), for instance, the liquid–liquid transition is observed almost simultaneously with the crystallization at 35 wt %. At higher concentrations liquid–liquid transition is observed a few degrees above crystallization, but only up to certain concentrations. With the sample of 54 wt % polymer concentration liquid–liquid separation can no longer be observed. This phenomena can be related to Nishi's observation[11] of the local phase separation during crystallization; the noncrystalline components are rejected preferentially by growing crystals, the solvent concentration at the growth front may exceed the binodal concentration, resulting in binodal decomposition. In our case, the liquid–liquid phase separation

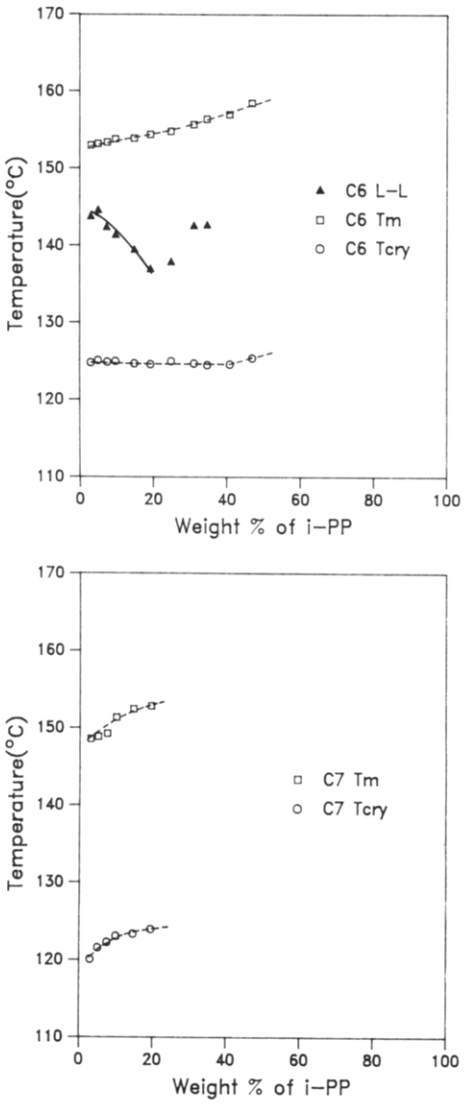


**Figure 5.** Experimental phase diagrams for the solutions of L-MW i-PP and $C_6$ (a, top) and $C_7$ (b, bottom) phthalates.

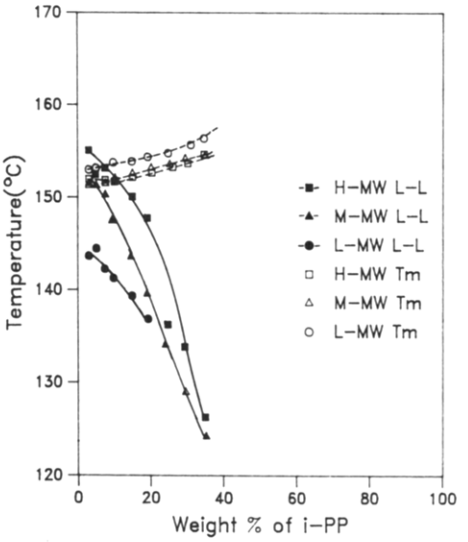


**Figure 6.** Liquid–liquid phase transitions and melting temperature curves for H-MW, M-MW, and L-MW i-PP with $C_6$ phthalate.

is due to similar local concentration fluctuations but occurs at the early stage of crystallization. In case of the L-MW sample, this liquid–liquid phase separation occurs at higher temperatures (earlier in time scale), as seen in Figure 5a.

**Table II**
**Effects of Solvent Quality and Polymer Molecular Weight on Phase Transitions[a]**

| solvent | H-MW i-PP | M-MW i-PP | L-MW i-PP |
|---|---|---|---|
| $C_4$ | $T_{L-L} > T_m$ | $T_{L-L} > T_m$ | $T_{L-L} > T_m$ |
| $C_6$ | $T_{L-L} > T_m$ | $T_{L-L} \sim T_m$ | $T_{L-L} < T_m$ |
| $C_7$ | $T_{L-L} < T_m$ | $T_{L-L} < T_m$ | $T_{L-L} < T_{cry}$ |
| $C_8$ | $T_{L-L} < T_m$ | $T_{L-L} < T_{cry}$ | $T_{L-L} < T_{cry}$ |
| $C_9$ | $T_{L-L} < T_{cry}$ | $T_{L-L} < T_{cry}$ | $T_{L-L} < T_{cry}$ |

[a] The comparison done at constant polymer concentration (5 wt %).

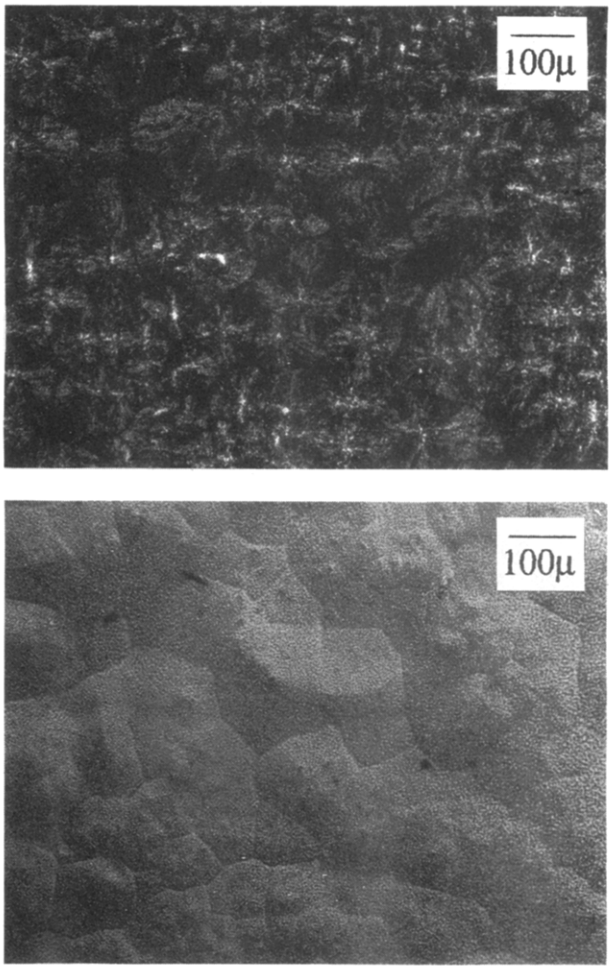


**Figure 7.** Optical micrographs of M-MW i-PP/$C_7$ (polymer concentration 20 wt %), cooled to 100 °C at 10 °C/min and held for 10 min: spherulitic structure under crossed polars (a, top) and with HMC (b, bottom).

It may be understood that the high diffusion rate of L-MW i-PP molecules gives rise to phase separation at earlier stages than in the cases of H-MW and M-MW fractions. The structures of the liquid–liquid phase separation induced by crystallization are shown in Figure 7 for a 20 wt % polymer concentration of M-MW i-PP/$C_7$ observed at 100 °C. Although this may also be detected by cloud point measurements, the visual observation through optical microscopy is essential to follow this liquid–liquid phase separation since the two transitions occur in a close temperature range.

**Liquid–Liquid Decomposition without Crystallization.** As shown above, we were not able to observe liquid–liquid phase separation before crystallization for the H-MW i-PP/$C_9$ pair at a cooling rate of 10 °C/min. A higher cooling rate than 10 °C/min is not applicable with our hot stage in an optical microscope. This has given us an inspiration to investigate the phase behavior of atactic

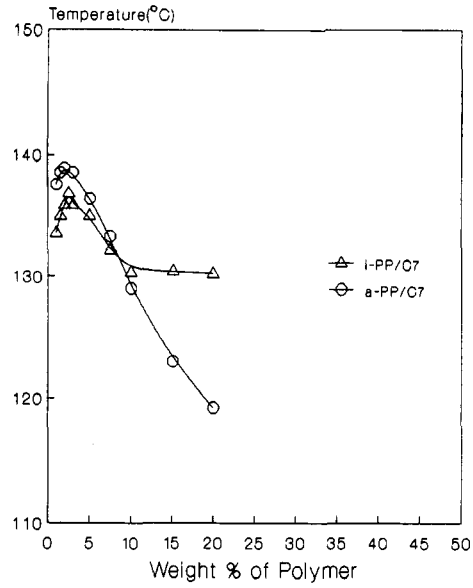


**Figure 8.** Liquid–liquid phase separation temperatures for i-PP/$C_7$ and a-PP/$C_7$ (at a cooling rate of 2 °C/min).

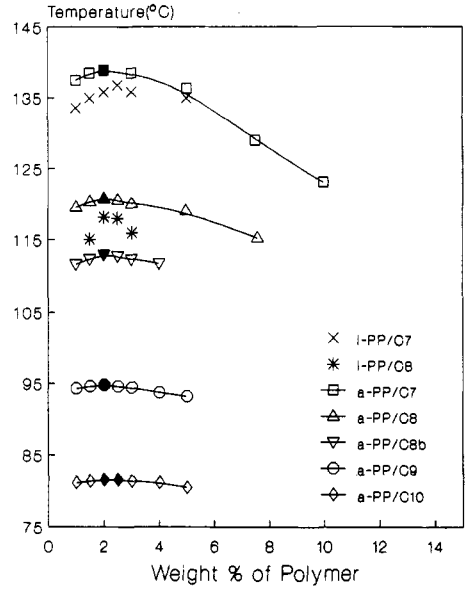


**Figure 9.** Liquid–liquid phase separation temperatures for i-PP/$C_7$, i-PP/$C_8$, a-PP/$C_7$, a-PP/$C_8$, a-PP/$C_{8b}$, a-PP/$C_9$, and a-PP/$C_{10}$ (at a cooling rate of 2 °C/min). The filled points represent the highest phase transition temperatures in the system.

polypropylene (a-PP) with the same solvents. The molecular weight of a-PP ($M_w$ 3.8 × $10^5$) in our experiments is in a region similar to that of i-PP ($M_w$ 3.1 × $10^5$). Liquid–liquid phase separation of a-PP is no more interfered with by crystallization since the a-PP is purely amorphous.

In Figure 8 the liquid–liquid phase separation temperatures are presented for both i-PP and a-PP using $C_7$ as the solvent. The peak temperature of liquid–liquid decomposition of the a-PP solution is a little higher, as is the molecular weight. The liquid–liquid phase separation outside the binodal region does not occur in the a-PP solution, because the phenomena is induced by crystallization under nonequilibrium conditions. The similar phase behavior with both i-PP and a-PP indicates that tacticity does not play an essential role. This suggests that we can use a-PP to probe the phase behavior of i-PP solutions.

Figure 9 shows the liquid–liquid phase separation temperatures for i-PP/$C_7$ and i-PP/$C_8$, which have been discussed earlier. Additionally, we have included the liquid–liquid decomposition temperatures for the a-PP

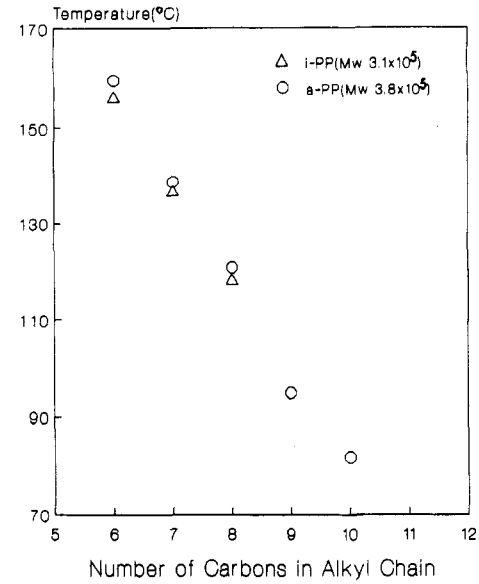


**Figure 10.** UCST (the highest liquid–liquid phase separation temperature) of the i-PP and the a-PP systems, as a function of solvent quality (at a cooling rate of 2 °C/min).

solutions with $C_7$, $C_8$, $C_{8b}$, $C_9$, and $C_{10}$. The decomposition temperatures decrease in a systematic manner when the solvent power is increased and crystallization does not disturb the measurements. Obviously, the appearance of UCST for a-PP/$C_{8b}$ at around 113 °C confirms our earlier morphological investigations[15] of the presence of liquid–liquid phase separation under high supercooling conditions. It is interesting to note that $C_{8b}$ (a branched alkyl chain) is a better solvent than $C_8$ (a linear alkyl chain) in Figure 9. This may be attributed to the alkyl chain configuration of the solvent molecules. The branched molecules may shield the polar ester group in the phthalate more effectively than the linear ones of the same carbon number.

The relationship between the highest liquid–liquid phase separation temperatures, which can be related to the UCST, and the number of carbons in the alkyl chain of the phthalate, which can be related to the solvent power, is presented in Figure 10. As the points for both a-PP and i-PP fit a straight line, respectively, it is clear that a liquid–liquid phase separation can occur at low temperatures in the i-PP systems unless crystallization interferes with liquid–liquid phase separation. Thus, a possible liquid–liquid phase separation, as in the cases of $C_9$ and $C_{10}$, can have a significant effect under high supercoolings on the resulting morphology in processing.

**Cooling Rate Effects.** All the above investigations were done with 10 °C/min cooling rates. It is of interest to investigate the influence of cooling rate on the interplay of the competitive phase transitions. Three different cooling rates were applied for the experiments; 10, 2, and 0.5 °C/min. The liquid–liquid phase separation temperatures for the M-MW i-PP/$C_6$ pair with the crystallization temperatures are shown in Figure 11 and for the M-MW i-PP/$C_7$ pair shown in Figure 12. The liquid–liquid decomposition temperatures shift to higher temperatures as slower cooling rates are applied. This reflects the kinetics of droplet formation due to liquid–liquid phase separation. The dependence of the UCST (the highest temperature of liquid–liquid decomposition) on the cooling rate for i-PP/$C_6$ and i-PP/$C_7$ systems is shown in Figure 13. The results may indicate that the measured values at slow cooling rates seem to deviate the linearity toward higher temperatures although the limited data make the analysis of the effect difficult. The extrapolated zero

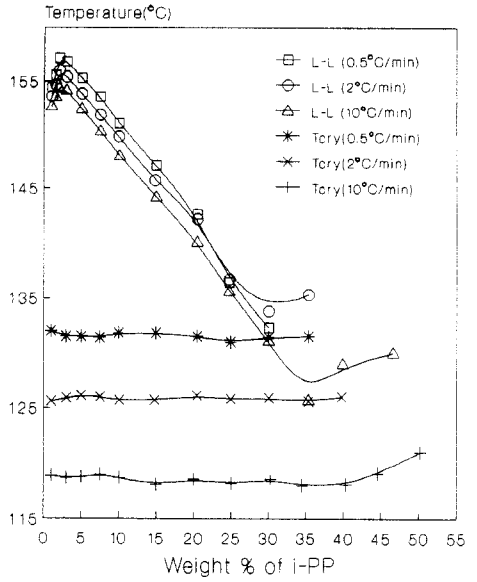


**Figure 11.** Liquid–liquid phase separation and crystallization temperatures for i-PP/$C_6$ with the different cooling rates.

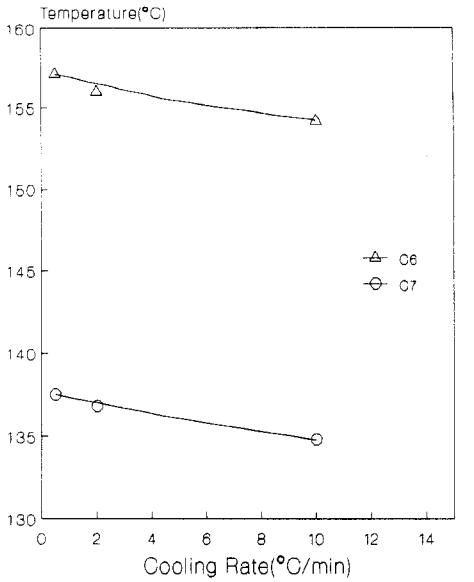


**Figure 13.** UCST (the peak temperatures of liquid–liquid phase transition) as a function of cooling rate for i-PP/$C_6$ and i-PP/$C_7$.

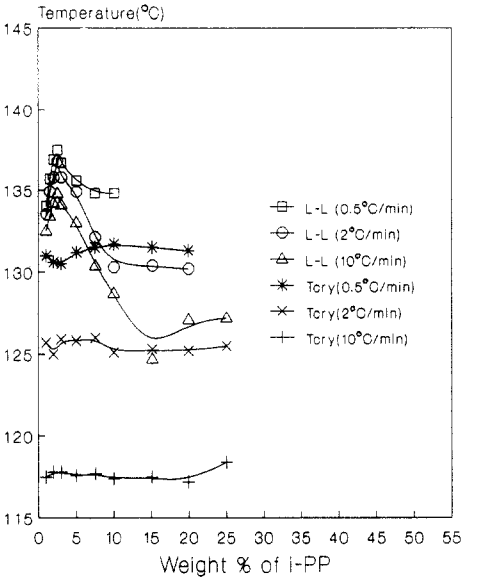


**Figure 12.** Liquid–liquid phase separation and crystallization temperatures for i-PP/$C_7$ with the different cooling rates.

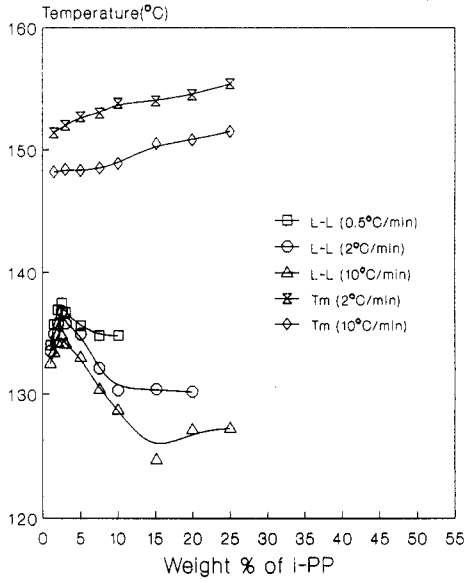


**Figure 14.** Melting and liquid–liquid phase separation temperatures for i-PP/$C_7$ with different heating and cooling rates.

cooling rate values represent the equilibrium upper critical solution temperatures. The experimental critical concentrations are approximately 2.0–2.5 wt % from Figures 11 and 12. The critical concentrations can also be estimated with the Flory-Huggins lattice model: the first and the second derivatives of chemical potential with respect to volume fraction of polymer are equal to zero at the critical point. Using a concentration-independent interaction parameter, we obtained the critical concentrations of about 2.5 wt %, similar to the experimental values.

The crystallization temperatures shift to higher temperatures with slower cooling rates. The shift to higher temperatures with decreased cooling rates is considerably larger in crystallization, showing that the nucleus formation in crystallization is more sensitive to supercooling than that in liquid–liquid phase separation. This reflects the difference in structure formation; the polymer chain should be packed more closely for crystal formation than for liquid droplet formation. The melting temperatures for the i-PP/$C_7$ solution with the liquid–liquid decomposition temperatures are shown in Figure 14. The liquid–liquid phase separation is clearly of a nonequilibrium nature, as these temperatures are all located below the melting temperatures. The melting temperature increases with the slower rate of heating, suggesting that lamellar thickening occurred during the heating process.

A liquid–liquid phase separation due to local concentration fluctuations can be observed outside the binodal region in Figures 11 and 12. The lower limit of polymer concentration for the M-MW/$C_7$ pair showing the phase separation, which is apparently related to crystallization, is different with the cooling rates: 15 wt % at 10 °C/min, 10 wt % at 2 °C/min, and 5 wt % at 0.5 °C/min. Thus a nonequilibrium liquid–liquid phase separation, which is induced by crystallization, is strongly dependent on the nonequilibrium conditions. The phase separations precede the crystallization by 7 °C at the rate of 10 °C/min, 5 °C at 2 °C/min, and 4 °C at 0.5 °C/min, as seen in Figure 12. It is understood that the solvent molecules can be segregated rapidly to give rise to phase separation under low supercooling (at an early stage of crystallization) before the birefringent crystals appear.

The effects of cooling rate on phase transitions in i-PP/$C_6$ (a worse solvent than $C_7$) follow trends similar to those in i-PP/$C_7$ (Figure 11). The liquid–liquid phase

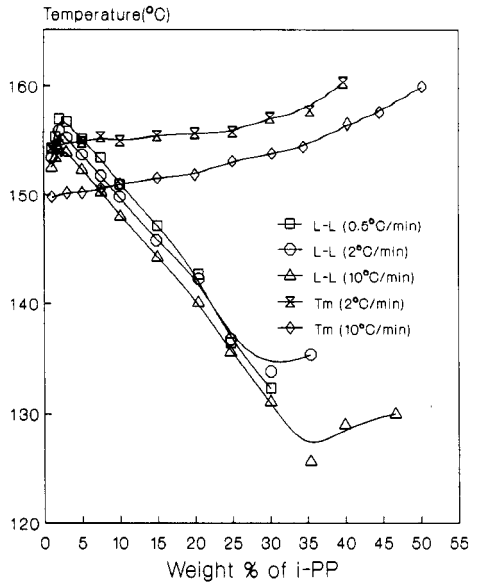


**Figure 15.** Melting and liquid–liquid phase separation temperatures for i-PP/$C_6$ with different heating and cooling rates.

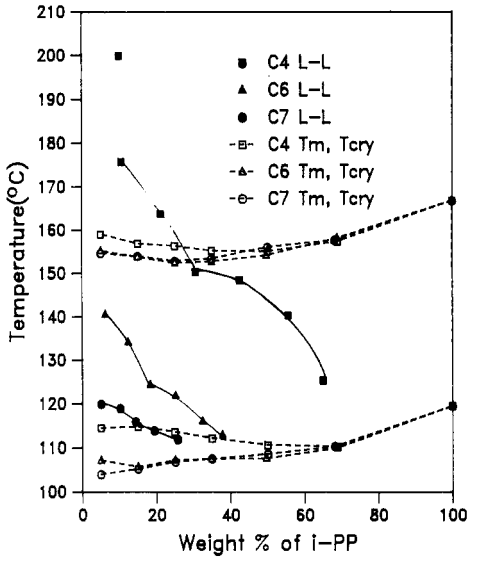


**Figure 16.** Liquid–liquid phase transition, crystallization, and melting curves for PD020 i-PP and $C_4$, $C_6$, and $C_7$ phthalate mixtures. Liquid–liquid phase transitions were obtained by optical microscopy and crystallization and melting temperatures measured by DSC.

separation appears again outside the binodal region. The liquid–liquid phase separation at 0.5 °C/min may be partly interpretated due to a smaller amount of solvents in the systems. Since the phase separation induced by crystallization occurs at a high concentration of i-PP, a greater portion of the solvents may be entrapped in the interlamellar region and the segregation to crystal growth front will be limited.

The melting temperatures rise with the slower heating rate in Figure 15. For 10 °C/min of cooling rate the liquid–liquid decomposition lies above the melting up to 7 wt %, and only to 3 wt % with the rate of 2 °C/min. At the rate of 0.5 °C/min, however, the liquid–liquid phase separation exists 1.5 °C below the melting (this point is not shown in Figure 15), which can be considered as a nonequilibrium liquid–liquid phase separation. These experiments manifest that an experimental phase diagram has to be analyzed with care due to the prevailing nonequilibrium conditions.

**Polydispersity Effects.** The phase behavior of a commercially available i-PP (PD020, Exxon) with a broad

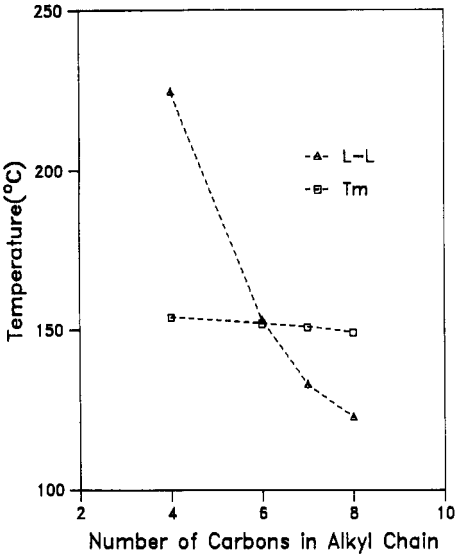


**Figure 17.** Relationship between $T_{L-L}$ and $T_m$ as a function of solvent quality (H-MW, i-PP, 5 wt %).

molecular weight distribution ($M_w/M_n$ 6.8) was also studied. The solvents $C_4$, $C_6$, and $C_7$ were used in the characterization of the liquid–liquid phase separation. The liquid–liquid phase transition and crystallization temperatures, both observed during the cooling cycle, are presented in Figure 16, in addition to the melting temperatures. Liquid–liquid transitions were observed by optical microscopy, and crystallization temperatures were obtained by DSC. It was impossible to determine the liquid–liquid phase separation temperatures precisely for the $C_4$ solution in concentrations below 20 wt % due to evaporation of the solvent. For 10 wt % $C_4$ solution the cloud point was observed to be 200 °C in a flask with solvent condensation.

An interesting feature is observed from the shapes of the liquid–liquid transition curves. All of the curves seem to have a bimodal shape at high concentrations. This behavior can be attributed to polydispersity of polymer molecules, and with a narrow molecular weight distribution specimen we do not observe this phenomena (as shown before). Another interesting feature is the elevation of crystallization and melting temperatures in liquid–liquid phase separation regions where these temperatures should remain constant according to the phase rule. The region of the crystallization temperature elevations is largest in the PD020 i-PP/$C_4$ sample where also the extent of liquid–liquid separation is greatest. The deviation of the constant $T_{cry}$ values decreases with $C_6$ and $C_7$ in which the regions of liquid–liquid phase separation are considerably lowered. The reason for this elevation of crystallization temperatures with dilution can be explained by fractionation effects on the polydisperse sample. During cooling, the high molecular weight fraction is phase-separated from the mother solution, and subsequently, the polymer-rich phase is crystallized. Thus the elevation of $T_{cry}$ values reflects the concentration of the precipitated phase. Similar elevation in vitrification curves due to polydispersity was recently reported by Vanderweerdt et al.[14] Neither the bimodal shape of the liquid–liquid transition nor the elevation of $T_m$ and $T_{cry}$ values were observed for the fractionated samples. This confirms the assumption that the above mentioned phenomena can be related to polydispersity.

In summary, the competition of liquid–liquid and liquid–solid phase separations depends on both the equilibrium phase behavior and the nonequilibrium conditions. The relations of the melting points and the liquid–liquid

phase transition temperatures with the solvent quality are shown in Figure 17, for a 5 wt % polymer concentration of H-MW i-PP. As the interaction becomes more favorable, the liquid–liquid phase separation temperature decreases remarkably and becomes a nonequilibrium transition when located below the melting curve. Although liquid–liquid phase transition in polymer solutions with favorable interaction cannot be observed in situ due to competing crystallization at slow cooling rates, it would play an important role on the resulting morphology under rapid quench to a low temperature.

**Acknowledgment.** We thank Dr. M. Wolkowicz in the Himont R&D Center and Dr. D. J. Lohse in Exxon Research and Engineering Co. for providing the polymer samples and L. G. Krauskopf at the Exxon Chemical Co. for the solvents.

## References and Notes

(1) (a) Castro, A. J. U.S. Patent 4,247,498, Jan 27, 1980. (b) Kesting, R. E. *Synthetic Polymeric Membranes, A Structural Perspective*; John Wiley and Sons: New York, 1985; p 261, (c) Lloyd, D. R. In *Materials Science of Synthetic Membranes*; Lloyd, D. R., Ed.; ACS Symposium Series No. 269; American Chemical Society: Washington, DC, 1985; p 1. (d) Strathman, H. Reference 1c, Vol. 8, p 165. (e) Hiatt, N. C.; Vitzthum, G. H.; Gerlach, K.; Wagener, K. B.; Josefiak, C. Reference 1c, Vol. 10, p 229. (f) Lloyd, D. R.; Barlow, J. W.; Kinzer, K. E. In *New Membrane Materials and Processes for Separation*; Sirkar, K. K., Lloyd, D. R., Eds.; AICHE Symposium Series 261; AICHE: New York, 1988. (g) Tsai, F. J.; Torkelson, J. M. *Macromolecules* **1990**, *23*, 775. (h) Caneba, G. T.; Soong, D. S. *Macromolecules* **1985**, *18*, 2545; 1985, *18*, 2538. (i) Lloyd, D. R.; Kinzer, K. E.; Tseng, H. S. *J. Membr. Sci.* **1990**, *52*, 239.

(2) (a) Doane, J. W.; Vaz, N. A.; Wu, B. G.; Zumar, S. *Appl. Phys. Lett.* **1986**, *48*, 269. (b) Doane, J. W. In *Liquid Crystals: Applications and Uses*; Balladur, B., Ed.; World Scientific Publishers: Teaneck, NJ, 1990; Chapter 14. (c) Doane, J. W.; Golemme, A.; West, J. L.; Whitehead, J. B., Jr.; Wu, B. G. *Mol. Cryst. Liq. Cryst.* **1989**, *165*, 511. (d) Doane, J. W. *MRS Bull.* **1991**, *16* (1), 22.

(3) Extensive review: *MRS Bull.* **1990**, *15*, 12.

(4) Richards, R. B. *Trans. Faraday Soc.* **1946**, *42*, 10.

(5) (a) Nakajima, A.; Hamada, F. *Kolloid Z. Z. Polym.* **1965**, *205*, 1. (b) Nakajima, A.; Fujiwara, H.; Hamada, F. J. *Polym. Sci.* **1966**, *A2* (4), 507. (c) Nakajima, A.; Fujiwara, H. *Polym. Sci.* **1968**, *A2*, (6), 723. (d) Flory, P. J.; Mandelkern, L.; Hall, H. K. *J. Am. Chem. Soc.* **1951**, *73*, 2532. (e) Bueche, A. M. *J. Am. Chem. Soc.* **1952**, *74*, 65. (f) Quinn, F. A.; Mandelkern, L. *J. Am. Chem. Soc.* **1958**, *80*, 3178.

(6) Koningsveld, R. On Liquid-Liquid Phase Relationships and Fractionation in Multicomponent Polymer Solutions. Ph.D. Thesis, University of Leiden, 1967.

(7) Chiu, G.; Mandelkern, L. *Macromolecules* **1990**, *23*, 5356.

(8) Burghardt, W. R. *Macromolecules* **1989**, *22*, 2482.

(9) Papkov, S. P.; Yefimova, S. G. *Vysokomol. Soedin.* **1966**, *8*, (11), 1984.

(10) Inaba, N.; Sato, K.; Suzuki, S.; Hashimoto, T. *Macromolecules* **1986**, *19*, 1690. Inaba, N.; Yamada, T.; Suzuki, S.; Hashimoto, T. *Macromolecules* **1988**, *21*, 407.

(11) Tanaka, H.; Nishi, T. *Phys. Rev. Lett.* **1985**, *55* (10), 1102; *Phys. Rev. A* **1989**, *39* (2), 783.

(12) Nojima, S.; Terashima, T.; Ashida, T. *Polymer* **1986**, *27*, 1007. Nojima, S.; Satoh, K.; Ashida, T. *Macromolecules* **1991**, *24*, 942.

(13) In order to obtain a narrow molecular weight distribution of a-PP, 2-methyl-1,3-pentadiene is polymerized anionically in the 1,4 mode. Subsequently, it is hydrogenated using a heterogeneous catalyst to more than 99% saturation.

(14) Vanderweerdt, P.; Berghmans, H.; Tervoort, Y. *Macromolecules* **1991**, *24*, 3547.

(15) Levon, K.; Karasz, F. E.; Lopatin, G.; Yen, L. Submitted for publication to *J. Polym. Sci., Polym. Phys. Ed.*

**Registry No.** PD020, 25085-53-4; a-PP, 9003-07-0; $C_4$, 84-74-2; $C_6$, 84-75-3; $C_7$, 3648-21-3; $C_8$, 117-81-7; $C_{8b}$, 117-81-7; $C_9$, 84-76-4; $C_{10}$, 84-77-5.